Nanoscale Advances

ROYAL SOCIETY OF CHEMISTRY

PAPER

View Article Online
View Journal | View Issue

Cite this: *Nanoscale Adv.*, 2025, **7**, 6084

Ferrocene-based covalent organic framework-carbon nanotube hybrid modified with $Cu(OAc)_2$ as a robust catalyst for the preparation of tetrazoles

Zahra Alishahi,[a] Mohammad Ali Zolfigol, *[a] Saeid Azizian,*[b] Morteza Torabi[a] and Yanlong Gu [c]

The emergence of covalent organic framework-carbon nanotube hybrid composites (COF-CNT) has opened up a promising approach for the development of heterogeneous catalysis. In this research, a new ferrocene-based COF was wrapped onto the surface of a carbon nanotube and modified with $Cu(OAc)_2$ (denoted as FCOF-CNT-$Cu(OAc)_2$) for boosting the catalytic performance for the preparation of tetrazoles. Ferrocene segments played a decisive role in assisting $Cu(OAc)_2$ as catalytically active sites for the preparation of 5-substituted 1*H*-tetrazoles and acrylonitrile-linked tetrazoles. FCOF-CNT-$Cu(OAc)_2$ had a high specific surface area of 117 m^2 g^{-1}, which accelerated the catalytic process. Field emission scanning electron microscopy (FE-SEM) and transmission electron microscopy (TEM) analyses revealed that the catalyst was ordered with a tubular morphology and spherical COF grown on the outer surface of the CNT. This work presents FCOF-CNT-$Cu(OAc)_2$ as a superior catalyst toward the preparation of 5-substituted 1*H*-tetrazoles and acrylonitrile-linked tetrazole derivatives. Consequently, tetrazole derivatives were synthesized in short reaction times under green and mild reaction conditions.

Received 9th June 2025
Accepted 6th August 2025

DOI: 10.1039/d5na00566c

rsc.li/nanoscale-advances

Introduction

COFs, as highly crystalline porous organic materials, are assembled with strong covalently bound building blocks, and they hold promises in diverse academic studies and offer broad practical applications such as in energy conversion and storage,[1,2] gas adsorption and separation,[3,4] sensing,[5] drug delivery,[6] electronic devices,[7] semiconductors,[8] and catalysis.[9] The outstanding characteristics of COFs include large specific surface area, well-defined porosity, low density, convenient functionalization, post-modification ability, and high thermal, chemical, and physical stabilities, each of which is of immense importance in the context of the applications of these materials.[10,11] In the context of catalytic applications of COFs, these are fantastic candidates in most catalytic processes such as asymmetric synthesis and photocatalytic, oxidation, reduction, coupling, and multicomponent reactions.[12–15] Due to the adjustable functionality of cavities, well-defined porosities, and rich metal chelation sites, these materials are rational and versatile hosts for metal ions, nanoparticles, and metal clusters.[16,17] A huge variety of reactions, such as the aryl methanol oxidation-aldol reaction,[18] click reaction-induced triazole synthesis,[19] Suzuki–Miyaura cross-coupling reaction[20] and Betti reaction,[21] have been facilitated by metal-ion-doped COFs. Cu(II)-coordinated COFs, because of their high activity, selectivity and ease of recovery and reusability, have a promising outlook and a decisive role in several catalytic reactions.[22–24]

Copper ions, due to their high selectivity and activity, natural abundance, and low cost, have garnered significant interest in catalytic transformations such as organometallic catalysis, gas-phase catalysis and photocatalysis.[25,26] Hereof, $Cu(OAc)_2$ nanoparticles is a paradigm example of click chemistry and is regarded as one of the most important synthetic trends for the preparation of heterocyclic compounds such as tetrazoles. Due to its broad applicability, selectivity, and biocompatibility, $Cu(OAc)_2$ plays a decisive role in the click chemistry preparation of tetrazole families.[27,28]

Recently, hybrid COFs such as COF-CNT,[29] COF-graphene oxide,[30] and COF-metal organic frameworks[31] have been reported. Among these, COF-CNT can solve some drastic problems like metal guest colonization, poor stability, and weak effective interactions.[32] Due to the strong π–π interactions between the COF layers and MVCNT, this complex can be a fantastic host for the decoration of metal ions as highly active catalytic centers.[33,34]

Ferrocene, as an interesting and unique functional moiety, has a distinctive electron-rich sandwich-like structure, which has inherent catalytic activity and is stable under harsh reaction

[a]*Department of Organic Chemistry, Faculty of Chemistry and Petroleum Sciences, Bu-Ali Sina University, Hamedan, Iran. E-mail: mzolfigol@yahoo.com; zolfi@basu.ac.ir*

[b]*Department of Physical Chemistry, Faculty of Chemistry and Petroleum Sciences, Bu-Ali Sina University, Hamedan, Iran. E-mail: sdazizian@yahoo.com*

[c]*School of Chemistry and Chemical Engineering, Huazhong University of Science and Technology, 1037 Luoyu Road, Hongshan District, Wuhan 430074, China*

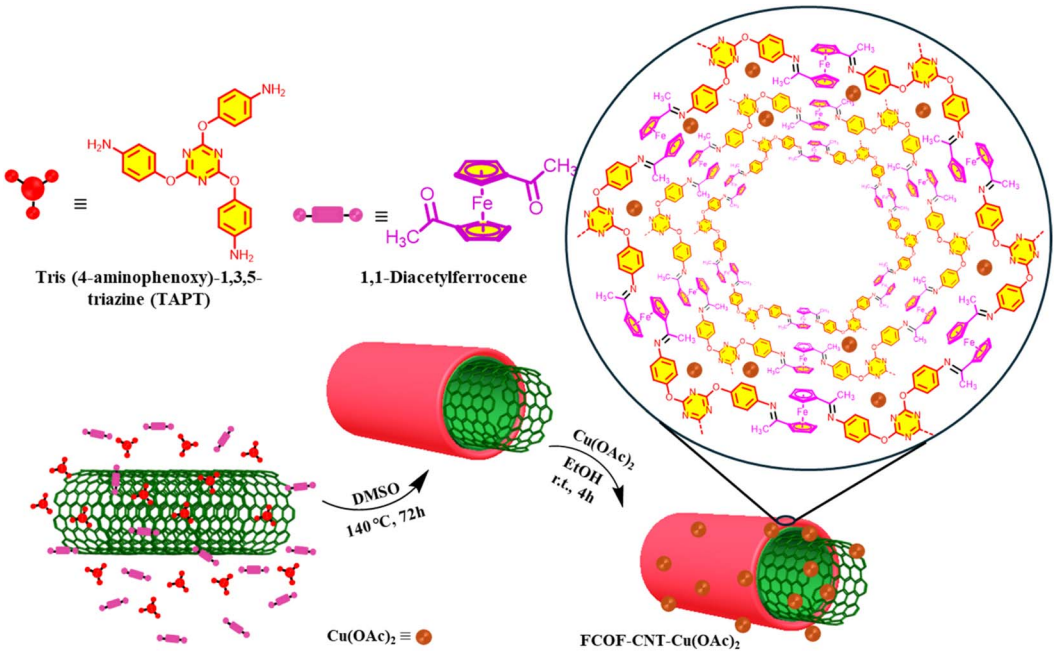

Scheme 1 Schematic of the fabrication of FCOF-CNT-Cu(OAc)$_2$.

conditions such as high temperature and alkaline and acidic media.[35] In recent years, ferrocene derivatives have been exploited as privileged building components for the fabrication of COFs.[36,37] Due to the organic–inorganic characteristics of ferrocene-based COFs and their superior performance as catalysts, they have been ingeniously applied in several catalytic

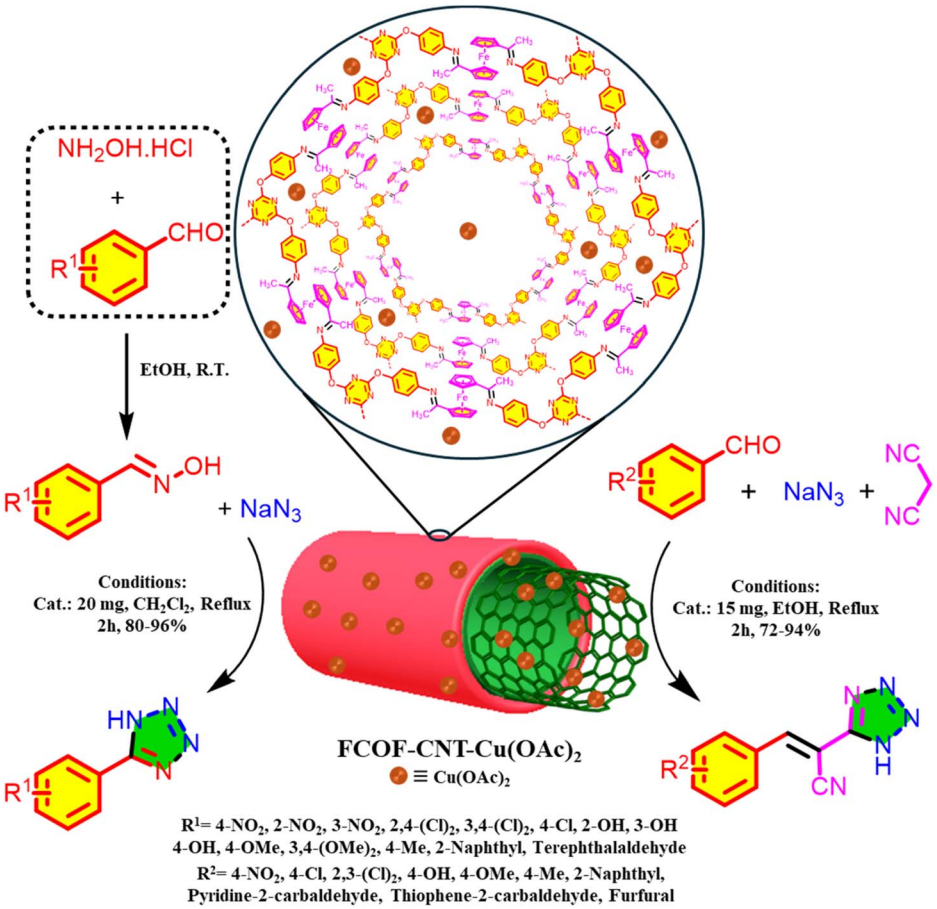

Scheme 2 Catalytic preparation of tetrazole derivatives using FCOF-CNT-Cu(OAc)$_2$.

reactions such as photocatalytic,[38] electrocatalytic,[39] and Fenton-like[40] reactions.

Heterocyclic chemistry is the heart of organic chemistry, and its catalytic synthesis has gained wide attention.[41] Chemicals containing tetrazoles are some of the most important and beneficial compounds belonging to the family of *N*-rich heterocycles, attracting burgeoning attention owing to their plethora of applications in functional materials, coordination chemistry, energetic materials, sensing, catalysis, and pharmaceuticals.[42–44] Several synthetic methodologies, such as 3 + 2 cycloaddition of nitriles and azides, cycloaddition of oximes and azides, and conversion of amides into tetrazole *via* the Mitsunobu reaction, have been reported for the preparation of tetrazoles.[45,46] In medicinal applications, tetrazole derivatives are known as anti-inflammatory, antibiotic, antihypertensive, antiallergic, antifungal, anti-HIV, and anticonvulsant agents and bioisosteres.[47–49] Among the tetrazole-bearing compounds, nitrile-linked tetrazoles have been neglected in the past century because of a lack of practical synthetic methods.[50] Therefore, development of suitable and applicable synthetic methodologies for these compounds requires great attention.

In this experimental study, considering our experience in porous materials, especially COFs,[51] a new ferrocene-based COF was fabricated on the surface of MVCNT and modified with $Cu(OAc)_2$. This catalytic platform was engineered with a predetermined goal in mind. We envisioned that the synergistic effects of the ferrocene core, CNT, and $Cu(OAc)_2$ in FCOF-CNT-$Cu(OAc)_2$ would make it an ideal catalyst for the preparation of tetrazole-based compounds (Schemes 1 and 2).

Results and discussion

Structural investigation of FCOF-CNT-$Cu(OAc)_2$

FT-IR and XRD analyses were adopted to explore the successful construction of FCOF-CNT-$Cu(OAc)_2$. The FT-IR spectra of the starting materials and intermediates at different steps of the catalyst synthesis are illustrated in Fig. 1, with the corresponding functional groups indicated. The carbonyl and cyclopentadienyl groups of 1,1-diacetylferrocene appeared at 1661 and 1459 cm^{-1}, respectively. In the FT-IR spectrum of TAPT, the characteristic absorption bands at 1608 and 1503 cm^{-1} corresponded to imine and aromatic groups, respectively. Moreover, the sharp peaks at 3465 and 3376 cm^{-1} were related to the amine functional group. According to the FT-IR spectrum of FCOF-CNT, it was clear that the disappearance of the NH_2 bands in TAPT and carbonyl band in 1,1-diacetylferrocene was accompanied by the emergence of a C=N band at 1698 cm^{-1}, indicating a polycondensation reaction between TAPT and 1,1-diacetylferrocene.[52,53] In the FT-IR spectrum of $Cu(OAc)_2 \cdot H_2O$, the strong peak at about 1631 cm^{-1} and the broad peak at about 3458 cm^{-1} were attributed to the stretching vibration mode of the C=O of acetate groups and H_2O, respectively. After coordinating Cu^{2+}, the main peaks in the FT-IR spectrum of FCOF-CNT did not change apparently.

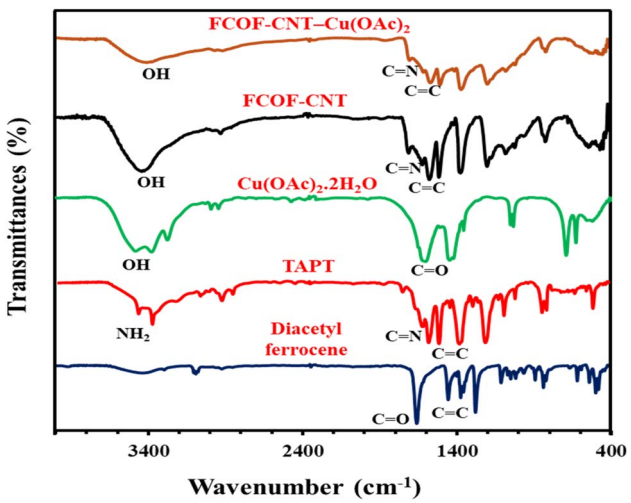

Fig. 1 FT-IR spectra of FCOF-CNT-$Cu(OAc)_2$ and its intermediates.

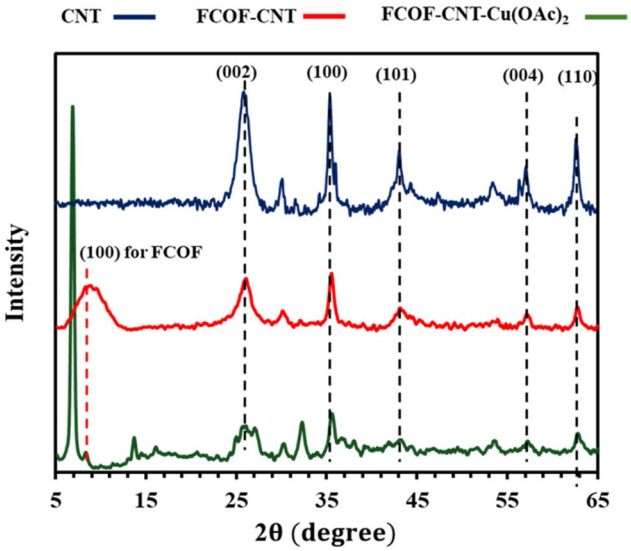

Fig. 2 XRD patterns of CNT, FCOF-CNT and FCOF-CNT-$Cu(OAc)_2$.

XRD patterns of CNT, FCOF-CNT and FCOF-CNT-$Cu(OAc)_2$ presented in Fig. 2 were used to evaluate the crystalline structure of FCOF-CNT-$Cu(OAc)_2$. The XRD pattern of CNT showed distinctive peaks at 26.2°, 35.6°, 43.3°, 57.3° and 62.8°, belonging to the (002), (100), (101), (004) and (110) planes, respectively. Besides, the XRD pattern of FCOF-CNT and FCOF-CNT-$Cu(OAc)_2$ displayed similar diffraction signals to that of CNT, indicating that the crystallinity of the CNT was retained after FCOF was wrapped on its surface. In the XRD pattern of FCOF-CNT, the (100) plane of FCOF was observed at 8.3°, indicating that the crystalline structure of FCOF was retained.[54] The XRD pattern of FCOF-CNT-$Cu(OAc)_2$ had additional peaks at 6.9°, 13.7° and 32.3°, indicating the successful loading of $Cu(OAc)_2$ while preserving the crystallinity of FCOF-CNT (Fig. 2).

Morphology investigation of FCOF-CNT-$Cu(OAc)_2$

According to FE-SEM analysis, FCOF-CNT-$Cu(OAc)_2$ exhibited a tubular morphology with spherical COF growths on the outer

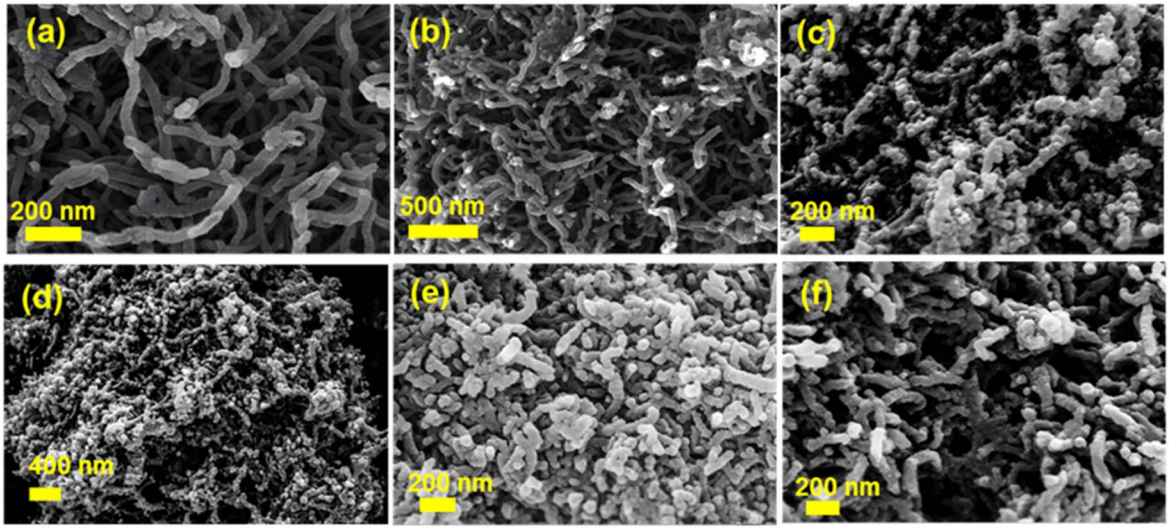

Fig. 3 FE-SEM images of CNT (a, b), FCOF-CNT (c, d) and FCOF-CNT-$Cu(OAc)_2$ (e, f).

surface of the CNT. As illustrated in Fig. 3a and b, the as-prepared CNT inherited a clean and regular nanotube structure with an average diameter of 40 nm, and its outer surface morphology was different from those of FCOF-CNT and FCOF-CNT-$Cu(OAc)_2$. The formation of spherical FCOF particles on the surface of CNT was observed in Fig. 3c–f, and the average diameter of FCOF-CNT-$Cu(OAc)_2$ was 70 nm, whose larger diameter and coarser surface can be attributed to the successful coating of FCOF on the surface of CNT. TEM analysis was used to further study the morphology of the catalyst. TEM images of FCOF-CNT and FCOF-CNT-$Cu(OAc)_2$ revealed the tubular morphology, in which the spherical FCOF was grown on the surface of CNT as core–shell structures (Fig. 4a–c). EDS analysis showed the predicted signals of C, N, O and Fe for FCOF-CNT and C, N, O, Cu and Fe for FCOF-CNT-$Cu(OAc)_2$ (Fig. 5). Mapping images revealed the uniform distribution of all the expected elements in both FCOF-CNT and FCOF-CNT-$Cu(OAc)_2$. Notably, the uniform distribution of Cu nanoparticles without any agglomeration was observed (Fig. 5).

Porosity evaluation of FCOF-CNT-$Cu(OAc)_2$

Porosity and surface area of FCOF-CNT and FCOF-CNT-$Cu(OAc)_2$ were investigated using the N_2 absorption–desorption isotherm and BET methods at 77 K. According to Fig. 6a and b, in the region of p/p_0 below 0.1, the N_2 adsorption of FCOF-CNT

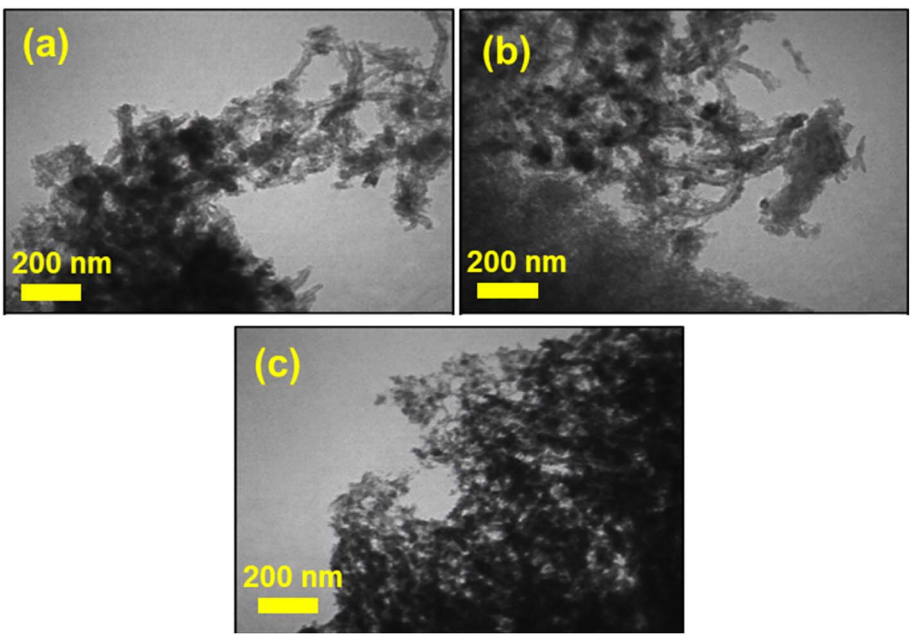

Fig. 4 TEM images of FCOF-CNT (a, b) and FCOF-CNT-$Cu(OAc)_2$ (c).

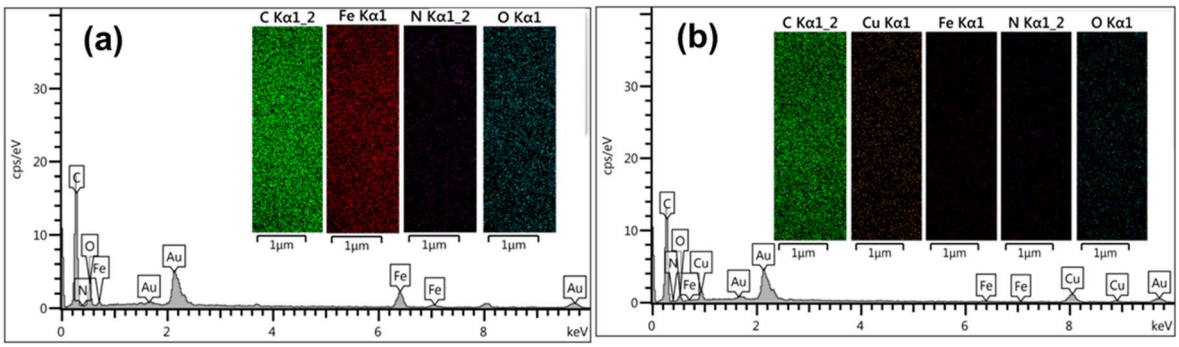

Fig. 5 EDS mapping results of FCOF-CNT (a) and FCOF-CNT-$Cu(OAc)_2$ (b).

was significantly increased, whereas the N_2 adsorption of FCOF-CNT-$Cu(OAc)_2$ increased at a gentler rate. This indicated the presence of more micropores in FCOF-CNT than in FCOF-CNT-$Cu(OAc)_2$, which can be attributed to the occupation of micropores by $Cu(OAc)_2$. By increasing the p/p_0 to 0.9, we observed hysteresis loops for both the samples, indicating the presence of a mesoporous structure for both of them. Moreover, the obtained BET surface area of FCOF-CNT and FCOF-CNT-$Cu(OAc)_2$ were 441 and 117 $m^2\ g^{-1}$, respectively. The Barrett–Joyner–Halenda (BJH) method was applied to show the pore size distributions in the samples. As illustrated in Fig. 6c and d, most of the pore radii for both FCOF-CNT and FCOF-CNT-$Cu(OAc)_2$ were less than 10 nm, indicating microporous and mesoporous structures.

Thermal stability analysis

TGA/DTG analysis with a heating rate of 10 °C min^{-1} was used to check the thermal stability of the catalyst. The TGA curves of FCOF-CNT and FCOF-CNT-$Cu(OAc)_2$ show only a small weight loss of 4% at about 70 °C, which can be attributed to the trapped

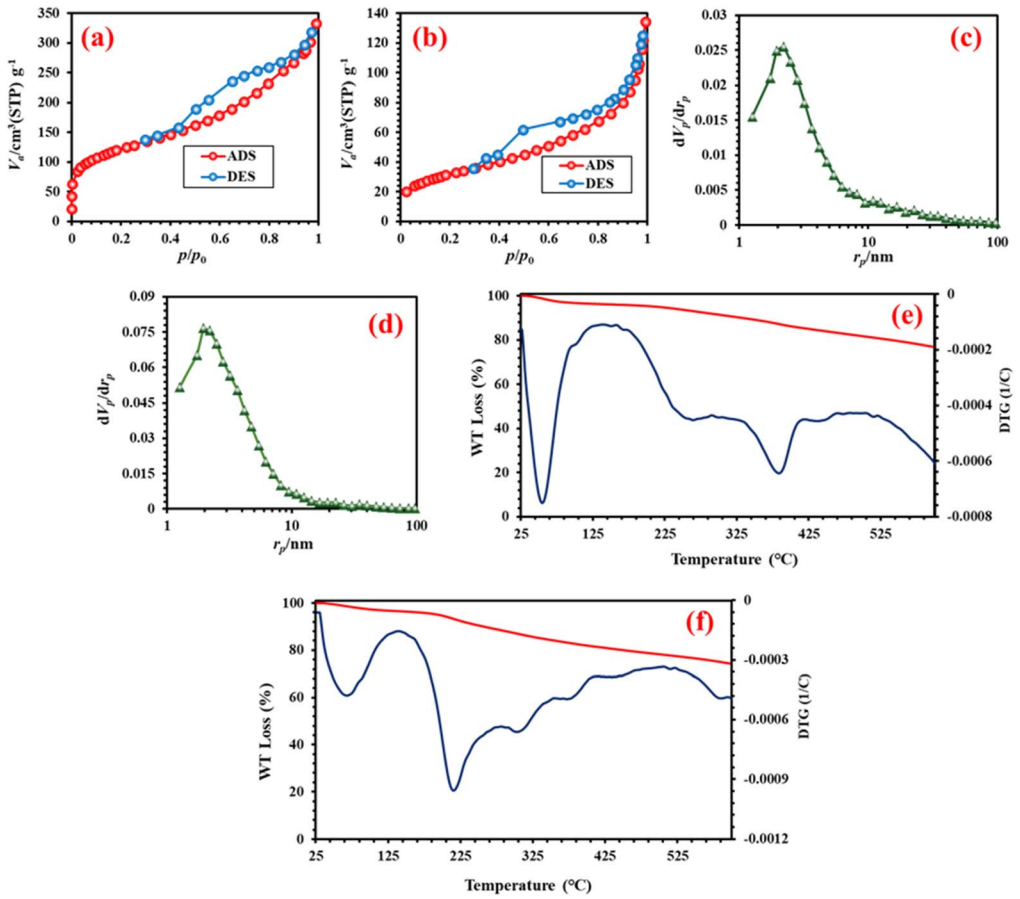

Fig. 6 N_2 adsorption/desorption isotherms of FCOF-CNT (a) and FCOF-CNT-$Cu(OAc)_2$. (b) Pore size distribution of FCOF-CNT (c) and FCOF-CNT-$Cu(OAc)_2$. (d) TGA/DTG curves of FCOF-CNT and (e) FCOF-CNT-$Cu(OAc)_2$ (f).

Table 1 Optimization of reaction conditions for the preparation of **1f** molecule[a]

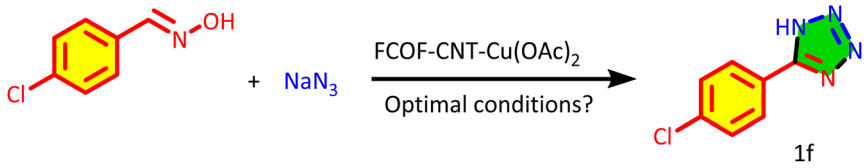

1f

Entry	Solvent	Temperature (°C)	Catalyst loading (mg)	Yield[b] (%)
1	CH_2Cl_2	Reflux	25	96
2	**CH_2Cl_2**	**Reflux**	**20**	**96**
3	CH_2Cl_2	Reflux	15	80
4	CH_2Cl_2	Reflux	10	30
5	CH_2Cl_2	Reflux	—	—
6	Water	Reflux	20	—
7	*n*-Hexane	Reflux	20	20
8	EtOH	Reflux	20	40
9	DMF	Reflux	20	94
10	MeOH	Reflux	20	—
11	—	110	20	—

[a] Reaction conditions: 4-chlorobenzaldehyde oxime (2 mmol, 0.312 g), sodium azide (3 mmol, 0.195 g), 2 h. [b] Isolated yield.

organic solvents, and another weight loss of 15% in the range of 200–400 °C may be ascribed to the removal of small portions of the organic layers and acetate groups of $Cu(OAc)_2$. In general, by increasing the temperature to 600 °C, approximately 20% of FCOF-CNT and FCOF-CNT-$Cu(OAc)_2$ was removed, confirming that both samples have excellent thermal stability (Fig. 6e and f).

Catalytic application of FCOF-CNT-$Cu(OAc)_2$

After precise characterization and analysis of FCOF-CNT-$Cu(OAc)_2$, we delved into its catalytic application for the preparation of tetrazoles. First of all, we tried to find the optimal reaction conditions for the preparation of 5-substituted 1*H*-tetrazoles and acrylonitrile-linked tetrazoles, separately. We chose the preparation of **1f** molecule as a model reaction using 4-chlorobenzaldehyde oxime and sodium azide as the starting materials. The main parameters, such as the solvent and amount of the catalyst, were evaluated. Therefore, the model reaction was performed with different solvents, including CH_2Cl_2, water, *n*-hexane, EtOH, MeOH, and DMF, under reflux conditions or solvent-free conditions at 110 °C. We found that performing the reaction with CH_2Cl_2 gave a better yield than using other solvents or under solvent-free conditions. Moreover,

Table 2 Optimization of reaction conditions for the preparation of **2b** molecule[a]

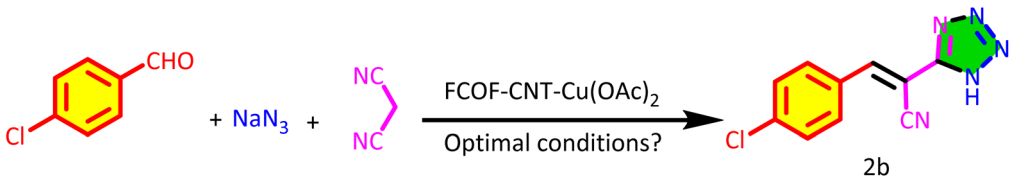

2b

Entry	Solvent	Temperature (°C)	Catalyst loading (mg)	Yield[b] (%)
1	EtOH	Reflux	20	94
2	**EtOH**	**Reflux**	**15**	**94**
3	EtOH	Reflux	10	85
4	EtOH	Reflux	—	—
5	Water	Reflux	15	30
6	*n*-Hexane	Reflux	15	40
7	EtOAc	Reflux	15	70
8	CH_2Cl_2	Reflux	15	Trace
9	MeOH	Reflux	15	80
10	—	110	15	—

[a] Reaction conditions: 4-chlorobenzaldehyde (2 mmol, 0.282 g), malononitrile (2.4 mmol, 0.158 g), sodium azide (3 mmol, 0.195 g), 2 h. [b] Isolated yield.

in most reported papers the reflux within the DMF and DMSO solvents were selected for the preparation of tetrazoles,[55] but we used the reflux of CH_2Cl_2 as a milder reaction condition, which is a key point in green chemistry and has more importance in saving energy resources. In addition, different amounts of catalyst were used for the model reaction, and 20 mg of FCOF-CNT-Cu(OAc)$_2$ was selected as the optimum amount of catalyst. The results, including further details, are listed in Table 1. In a similar study, we realized that the optimized reaction conditions for the preparation of acrylonitrile-linked tetrazoles were using EtOH as the solvent under reflux conditions, and 15 mg FCOF-CNT-Cu(OAc)$_2$ was the optimum amount of catalyst (Table 2).

With the optimum conditions and promising results in hand, a series of aldehydes and aldehyde oximes were subjected to the synthesis of acrylonitrile-linked tetrazoles and 5-substituted-1*H*-tetrazoles, respectively. Diverse electron-donating and electron-withdrawing substituted aldehydes and aldehyde oximes were applied, and good results were obtained. All derivatives were synthesized in short reaction times (2 h) with high yields (80–96% for 5-substituted-1*H*-tetrazoles and 72–94% for acrylonitrile-linked tetrazoles) (Tables 3 and 4). In another study, to verify the potential of FCOF-CNT-Cu(OAc)$_2$ as a highly active catalyst, we compared its activity with those of FCOF-CNT, CNT and Cu(OAc)$_2$ for the model reaction. The yield of **1f** was found to be significantly decreased with FCOF-CNT,

Table 3 Catalytic preparation of 5-substituted 1*H*-tetrazoles using the FCOF-CNT-Cu(OAc)$_2$ catalyst[a]

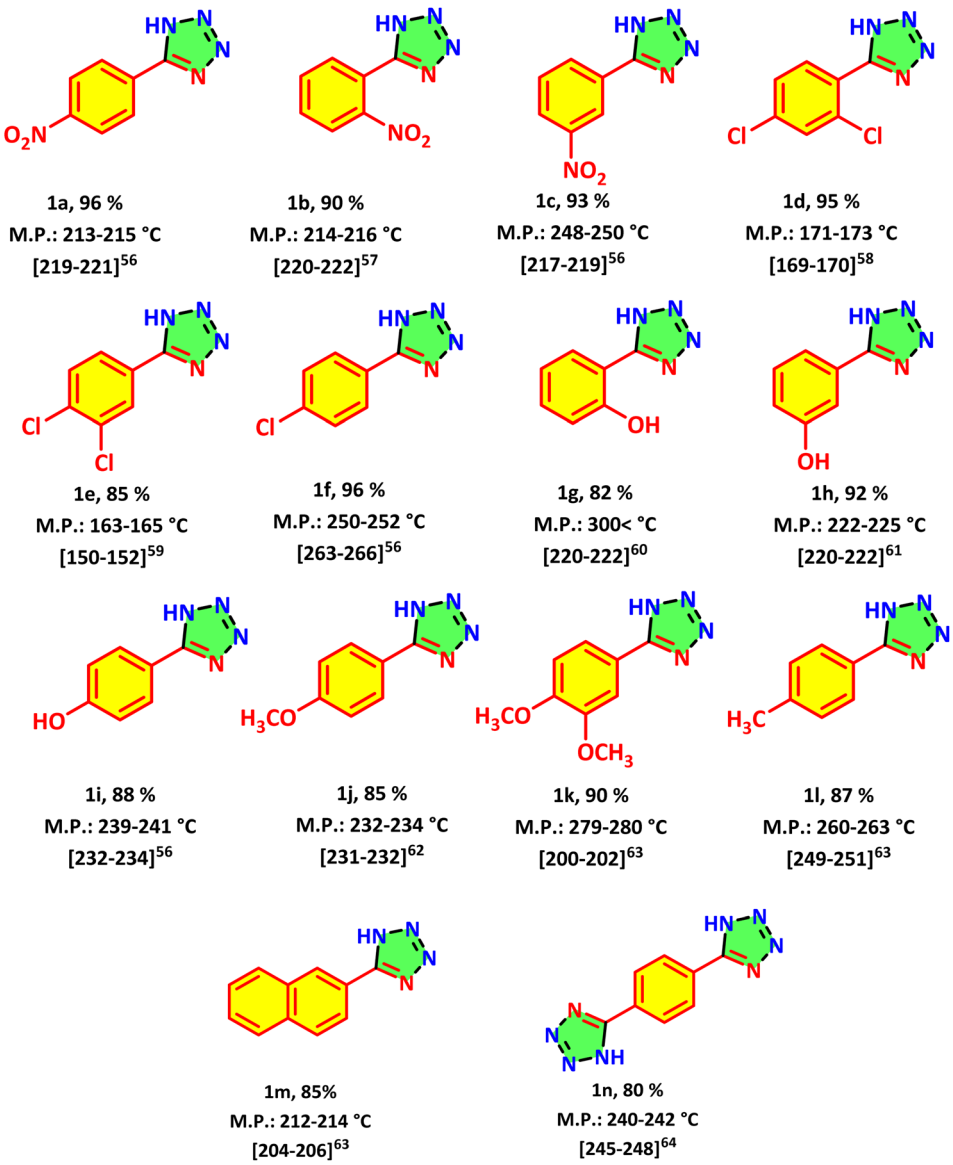

[a] Reaction conditions: aldehyde oxime (2 mmol), sodium azide (3 mmol, 0.194 g), CH_2Cl_2, reflux, 40 °C, 2 h, catalyst (20 mg), reported yields are isolated yields.[56–64]

Table 4 Catalytic preparation of acrylonitrile-linked tetrazoles using the FCOF-CNT-Cu(OAc)$_2$ catalyst[a]

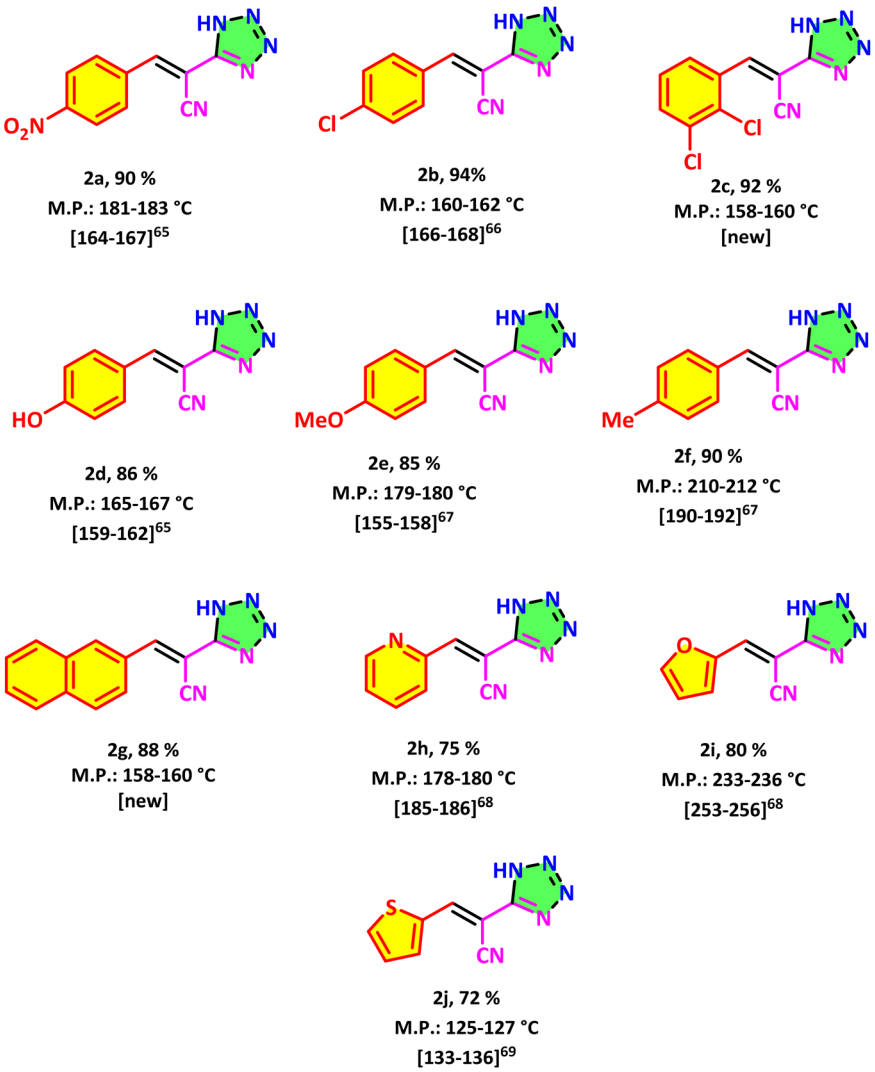

[a] Reaction conditions: aldehyde (2 mmol), sodium azide (3 mmol, 0.195 g), malononitrile (2.4 mmol, 0.158 g), EtOH, reflux, 80 °C, 2 h, catalyst (15 mg), reported yields are isolated yields.[65–69]

Table 5 Comparison of the catalytic ability of FCOF-CNT-Cu(OAc)$_2$, FCOF-CNT, CNT and Cu(OAc)$_2$ for the preparation of **1f**[a]

Entry	Catalyst	Catalyst loading	Yield (%)
1	**FCOF-CNT-Cu(OAc)$_2$**	**20 mg**	**96**
2	COF-CNT	20 mg	40
3	CNT	20 mg	20
4	Cu(OAc)$_2$	10 mol%	30

[a] Reaction conditions: 4-chlorobenzaldehyde oxime (2 mmol, 0.312 g), sodium azide (3 mmol, 0.195 g), 2 h, CH_2Cl_2, reflux, 40 °C.

CNT and Cu(OAc)$_2$ as catalysts rather than FCOF-CNT-Cu(OAc)$_2$ (Table 5).

In addition, in a comparative study, the catalytic activity of FCOF-CNT-Cu(OAc)$_2$ and some of the reported homogeneous and heterogeneous catalysts was evaluated for the preparation of **1f** molecule. According to the revealed results, FCOF-CNT-Cu(OAc)$_2$ exhibited a higher catalytic activity under milder reaction conditions than most of the reported catalysts. We note that the recyclability and reusability of FCOF-CNT-Cu(OAc)$_2$ is a crucial parameter that makes it more valuable than homogeneous catalysts (Table 6).

To examine the recovery and reusability of the catalyst, recycling tests with FCOF-CNT-Cu(OAc)$_2$ were conducted for the preparation of **2b** under the optimal reaction conditions. After completing the reaction, CH_2Cl_2 was added to the flask and insoluble FCOF-CNT-Cu(OAc)$_2$ was separated from the reaction mixture *via* filtration, washed with CH_2Cl_2, dried at 100 °C and retained for the next run. The catalytic ability of FCOF-CNT-Cu(OAc)$_2$ was well preserved after six consecutive reaction cycles, and no significant loss in catalytic performance was

Table 6 Comparison of the catalytic ability of FCOF-CNT-$Cu(OAc)_2$ with some reported heterogeneous and homogeneous catalysts for the preparation of **1f**

Entry	Catalyst	Time (h)	Yield (%)
1	**FCOF-CNT-$Cu(OAc)_2$, CH_2Cl_2, reflux, 40 °C, [this work]**	**2**	**96**
2	Diphenyl phosphorazidate, toluene, reflux[49]	16	89
3	25 mol% $Cu(OAc)_2$, DMF, 120 °C (ref. 44)	12	90
4	CoY zeolite, DMF, 120 °C (ref. 48)	14	91
5	Pincer type Pd(II) complex, KOH, H_2O/DMSO, 90 °C (ref. 70)	8	78
6	(η^6-*p*-cymene)Ruthenium(II), DMF, 140 °C (ref. 71)	8	93
7	$CuSO_4 \cdot 5H_2O$, DMSO, 140 °C (ref. 55)	0.5	100
8	$AgNO_3$, DMF, 120 °C (ref. 55)	5	80
9	Piperazinium hydrogensulfate, 100 °C (ref. 72)	2	93
10	Copper-coordinated-poly(α-amino acid)/magnetite graphene oxide, water, 70 °C (ref. 47)	1.41	92

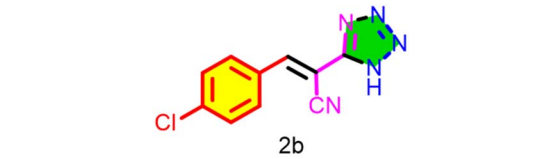

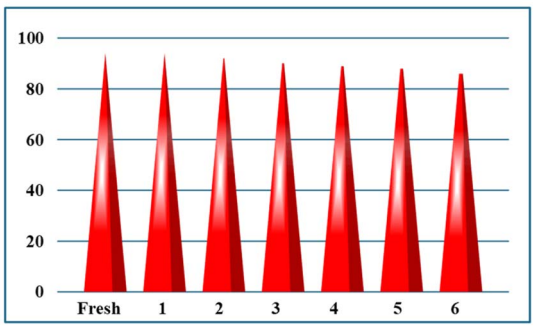

Run	Fresh	1	2	3	4	5	6
Isolated yields (%)	94	94	92	90	89	88	86

Scheme 3 Recoverability and reusability of COF-CNT-$Cu(OAc)_2$.

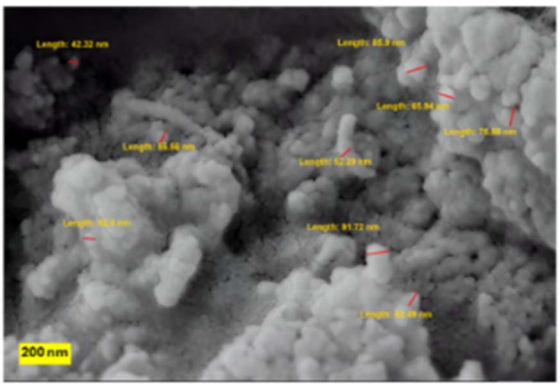

Fig. 7 FE-SEM image of recovered COF-CNT-$Cu(OAc)_2$.

observed (Scheme 3). The FE-SEM and EDS/mapping analyses results of the recovered catalyst are shown in Fig. 7 and 8.

Inspired by a previous report,[44] we suggest a plausible mechanism for the preparation of tetrazoles (Scheme 4). First, the hydroxy group of the oxime is activated by the catalyst, which facilitates the nucleophilic attack and cycloaddition of NaN_3 across the C=N group. In the next step, the desired product is generated by removing H_2O, assisted by the catalyst, as well as hydrolysis by acid.

Experimental section

In the Experimental section, the importance of a non-stoichiometric ratio of reactants in organic synthesis for delivering high yields of products was considered.[73]

Materials and methods

In this research, all starting materials and reagents were purchased from Merck and Sigma-Aldrich companies and were applied without further purification. FT-IR spectra were recorded with an FT-IR spectrometer, PerkinElmer Spectrum 65 model. ^{1}H NMR spectra were performed on a Bruker spectrometer operating at 250 MHz, and ^{13}C NMR spectra were performed at 62 MHz. FE-SEM analysis was performed with a TESCAN MIRA4 instrument, and TEM analysis was conducted with a ZEISS, EM10C-100 KV instrument. X-ray diffraction (XRD) analysis was performed with an X'Pert Pro instrument. N_2 adsorption/desorption isotherms were obtained using a BELSORP Mini model instrument. Thermogravimetric/derivative thermogravimetry analysis (TGA/DTG) (Mettler Toledo company, TGA2 model) was used to investigate the thermal stability of the catalyst.

General experimental procedure for the synthesis of FCOF-CNT-$Cu(OAc)_2$. The synthetic procedure for FCOF-CNT-$Cu(OAc)_2$ is shown in Scheme 1. 1,1-Diacetylferrocene (1.5 mmol, 0.405 g), tris(4-aminophenoxy)-1,3,5-triazine (TAPT) (1 mmol, 0.402 g), CNT (0.2 g) and DMSO (30 mL) were added to a round-bottom flask, and the reaction mixture was refluxed for 72 h at 140 °C under an N_2 atmosphere. After completing the reaction, the obtained FCOF-CNT was filtered and washed several times with MeOH and tetrahydrofuran (THF) and finally dried at 120 °C for 24 h. FCOF-CNT (0.5 g), $Cu(OAc)_2 \cdot H_2O$ (0.75 mmol, 0.15 g), and 30 mL of dry ethanol were then stirred at room temperature for 4 h. The resulting product was washed with ethanol and placed in an oven at 120 °C for 12 h to remove any trapped solvents.

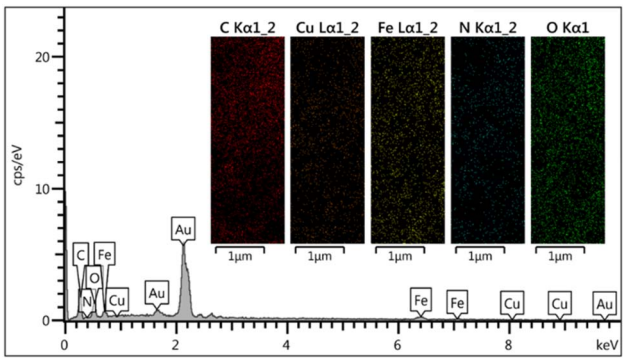

Fig. 8 EDS signals and mapping images of recovered COF-CNT-$Cu(OAc)_2$.

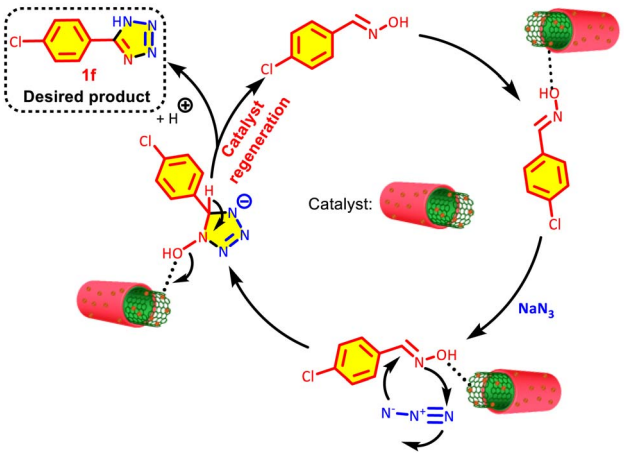

Scheme 4 Plausible mechanism for the preparation of **1f** molecule.

Synthesis of 5-substituted 1H-tetrazoles in the presence of FCOF-CNT-Cu(OAc)$_2$. Initially, to prepare the oxime derivatives, a mixture of aromatic aldehydes (2 mmol), pyridine (3 mmol, 0.237 g) as catalyst, and hydroxylamine hydrochloride (3 mmol, 0.208 g) and 10 mL of ethanol were poured into a round-bottomed flask and stirred at room temperature for 6 h. After that, the formed solids were washed by water to yield the desired pure product. In the next step, oxime derivatives (2 mmol), sodium azide (3 mmol, 0.195 g) and 20 mg FCOF-CNT-$Cu(OAc)_2$ as catalyst were added to 10 mL of CH_2Cl_2 and refluxed at 40 °C. After completion of the reaction, the catalyst was separated using a filtration method. After removing the solvent, 10 mL of 2 M hydrochloric acid was added to the reaction mixture, and the resulting precipitate was washed with water and EtOH to obtain the pure product.

Synthesis of acrylonitrile-linked tetrazole derivatives using FCOF-CNT-Cu(OAc)$_2$ catalyst. A mixture of aromatic aldehyde (2 mmol), sodium azide (3 mmol, 0.195 g), malononitrile (2.4 mmol, 0.158 g), FCOF-CNT-$Cu(OAc)_2$ (15 mg) and EtOH (10 mL) was added to a 10 mL round-bottomed flask and stirred at 80 °C. Upon completion of the reaction, 20 mL of CH_2Cl_2 was added to the flask and the insoluble catalyst was separated using filtration. The solvent was removed, and 10 mL of 2 M hydrochloric acid was added to the reaction mixture and the resulting precipitate was washed with water and cold EtOH to yield the pure acrylonitrile-linked tetrazole derivative.

Spectral data

5-(4-Nitrophenyl)-1*H*-tetrazole. M.p. = 213–215 °C, FT-IR (KBr, ν, cm^{-1}): 3447, 3219, 1552, 1515, 1339. ^{1}H NMR (250 MHz, DMSO-d_6) δ_{ppm} 8.41 (d, J = 7.5 Hz, 2H), 8.27 (d, J = 7.5 Hz, 2H). ^{13}C NMR (63 MHz, DMSO-d_6) δ_{ppm} 149.1, 131.1, 128.7, 125.0.

5-(3-Nitrophenyl)-1*H*-tetrazole. M.p. = 248–250 °C, FT-IR (KBr, ν, cm^{-1}): 3159, 2955, 1602, 1574, 1321. ^{1}H NMR (250 MHz, DMSO-d_6) δ_{ppm} 9.82 (s, 1H), 7.69–7.32 (m, 2H), 6.89 (s, 1H). ^{13}C NMR (63 MHz, DMSO-d_6) δ_{ppm} 160.1, 154.0, 132.4, 124.4, 120.8, 117.9.

5-(2,4-Dichlorophenyl)-1*H*-tetrazole. M.p. = 171–173 °C, FT-IR (KBr, ν, cm^{-1}): 3421, 2918, 1614, 1570, 1505. ^{1}H NMR (250 MHz, DMSO-d_6) δ_{ppm} 7.96 (s, 1H), 7.39 (broad peak, 2H). ^{13}C NMR (63 MHz, DMSO-d_6) δ_{ppm} 141.5, 130.6, 127.8.

5-(4-Chlorophenyl)-1*H*-tetrazole. M.p. = 250–252 °C, FT-IR (KBr, ν, cm^{-1}): 3422, 3098, 1687, 1610. ^{1}H NMR (250 MHz, DMSO-d_6) δ_{ppm} 8.35 (s, 1H), 7.95 (s, 1H), 7.62 (s, 2H). ^{13}C NMR (63 MHz, DMSO-d_6) δ_{ppm} 155.2, 136.3, 130.0, 129.3, 123.7.

3-(1*H*-Tetrazol-5-yl)phenol. M.p. = 222–225 °C, FT-IR (KBr, ν, cm^{-1}): 3193, 3053, 1603, 1574, 1472. ^{1}H NMR (250 MHz, DMSO-d_6) δ_{ppm} 9.81 (s, 1H), 7.30 (broad peak, 3H), 6.87 (s, 1H). ^{13}C NMR (63 MHz, DMSO-d_6) δ_{ppm} 160.0, 132.3, 119.2, 118.6, 118.0.

5-(Naphthalen-2-yl)-1*H*-tetrazole. M.p. = 212–214 °C, FT-IR (KBr, ν, cm^{-1}): 3422, 3055, 1649, 1495. ^{1}H NMR (250 MHz, DMSO-d_6) δ_{ppm} 8.56–8.40 (m, 2H), 8.19–7.89 (m, 3H), 7.64–7.54 (m, 2H). ^{13}C NMR (63 MHz, DMSO-d_6) δ_{ppm} 148.6, 134.7, 132.9, 132.7, 130.4, 129.4, 129.1, 128.3, 127.8, 124.9.

1,4-Di(1*H*-tetrazol-5-yl)benzene. M.p. = 240–242 °C, FT-IR (KBr, ν, cm^{-1}): 3358, 3088, 1660, 1434. ^{1}H NMR (250 MHz, DMSO-d_6) δ_{ppm} 8.14–7.94 (m, 4H).

(*E*)-3-(4-Chlorophenyl)-2-(1*H*-tetrazol-5-yl)acrylonitrile. M.p. = 160–162 °C, FT-IR (KBr, ν, cm^{-1}): 3452, 3154, 2230, 1586. ^{1}H NMR (250 MHz, DMSO-d_6) δ_{ppm} 8.67 (s, 1H), 8.10–7.88 (m, 2H), 7.66–7.51 (m, 2H). ^{13}C NMR (63 MHz, DMSO-d_6) δ_{ppm} 147.3, 137.3, 131.9, 131.5, 129.8, 115.9, 98.4.

(*E*)-3-(2,3-Dichlorophenyl)-2-(1*H*-tetrazol-5-yl)acrylonitrile. M.p. = 158–160 °C, FT-IR (KBr, ν, cm^{-1}): 3422, 3141, 2233, 1610. ^{1}H NMR (250 MHz, DMSO-d_6) δ_{ppm} 8.57 (s, 1H), 8.00 (s, 1H), 7.84 (d, J = 7.5 Hz, 1H), 7.57 (s, 1H). ^{13}C NMR (63 MHz, DMSO-d_6) δ_{ppm} 144.3, 133.8, 133.4, 133.2, 132.07, 130.0, 129.3, 128.9, 115.0, 103.7.

(*E*)-3-(4-Hydroxyphenyl)-2-(1*H*-tetrazol-5-yl)acrylonitrile. M.p. = 165–167 °C, FT-IR (KBr, ν, cm^{-1}): 3334, 3172, 2233, 1599. ^{1}H NMR (250 MHz, DMSO-d_6) δ_{ppm} 10.49 (s, 1H), 8.19–7.87 (m, 3H), 6.89 (s, 2H). ^{13}C NMR (63 MHz, DMSO-d_6) δ_{ppm} 162.1, 148.9, 133.7, 132.9, 123.9, 117.5, 117.2, 92.4.

(*E*)-3-(Naphthalen-2-yl)-2-(1*H*-tetrazol-5-yl)acrylonitrile. M.p. = 158–160 °C, FT-IR (KBr, ν, cm^{-1}): 3422, 3141, 2233, 1610. ^{1}H NMR (250 MHz, DMSO-d_6) δ_{ppm} 8.57 (s, 1H), 8.00 (s, 1H), 7.84 (d, J = 7.5 Hz, 1H), 7.57 (s, 1H). ^{13}C NMR (63 MHz, DMSO-d_6) δ_{ppm}

144.3, 133.8, 133.4, 133.2, 132.1, 130.0, 129.3, 128.9, 115.0, 103.7.

Conclusion

To summarize, a $Cu(OAc)_2$-loaded ferrocene-based COF-wrapped MVCNT was evaluated as a hybrid-reticular catalyst. Benefiting from the synergistic effect of ferrocene moiety, CNT and $Cu(OAc)_2$, FCOF-CNT-$Cu(OAc)_2$ exhibited a superior and appropriate catalytic performance in multi-component reactions. More importantly, FCOF-CNT-$Cu(OAc)_2$ exhibited an ordered and tubular morphology, high porosity and great stability. Accordingly, FCOF-CNT-$Cu(OAc)_2$ was successfully assessed for the preparation of 5-substituted 1*H*-tetrazoles and acrylonitrile-linked tetrazoles. The synthesized tetrazole derivatives were prepared in high yields under short reaction times and mild reaction conditions compared with previous reports. In addition, this catalyst showed acceptable recovery and reusability, whereby its activity was well preserved after six consecutive reaction cycles with no significant loss in its catalytic potential. This study provides an intense insight into the key role of hybrid reticular chemistry-based catalysis in organic transformations and can encourage chemists to develop new hybrid COFs.

Author contributions

Zahra Alishahi: writing – original draft, validation, methodology, investigation. Mohammad Ali Zolfigol: writing – review & editing, project administration, resources, supervision, funding acquisition, conceptualization, data curation. Morteza Torabi: writing – original draft, validation, methodology, investigation. Yanlong Gu: resources, data curation, methodology.

Conflicts of interest

The authors declare no competing interests.

Data availability

The data supporting this article have been included as part of the SI. See DOI: https://doi.org/10.1039/d5na00566c.

Acknowledgements

We thank the Bu-Ali Sina University and Iran National Science Foundation (INSF) (Grant Number: 4041905) for providing the financial support to our research group.

References

1 M. Chafiq, A. Chaouiki and Y. G. Ko, Advances in COFs for energy storage devices: harnessing the potential of covalent organic framework materials, *Energy Storage Mater.*, 2023, **63**, 103014–103043.
2 X. Feng, X. Ding and D. Jiang, Covalent organic frameworks, *Chem. Soc. Rev.*, 2012, **41**, 6010–6022.
3 M. Liu, S. Yang, X. Yang, C. X. Cui, G. Liu, X. Li, J. He, G. Z. Chen, Q. Xu and G. Zeng, Post-synthetic modification of covalent organic frameworks for CO_2 electroreduction, *Nat. Commun.*, 2023, **14**, 3800.
4 G. O. Aksu and S. Keskin, The COF space: materials features, gas adsorption, and separation performances assessed by machine learning, *ACS Mater. Lett.*, 2025, **7**, 954–960.
5 X. Liu, D. Huang, C. Lai, G. Zeng, L. Qin, H. Wang, H. Yi, B. Li, S. Liu, M. Zhang, R. Deng, Y. Fu, L. Li, W. Xue and S. Chen, Recent advances in covalent organic frameworks (COFs) as a smart sensing material, *Chem. Soc. Rev.*, 2019, **48**, 5266–5302.
6 M. J. Kang, Y. W. Cho and T. H. Kim, Metal- and covalent-organic framework-based drug delivery systems: applications to control cell functions, *Coord. Chem. Rev.*, 2025, **527**, 216400–216440.
7 M. D. Allendorf, R. Dong, X. Feng, S. Kaskel, D. Matoga and V. Stavila, Electronic devices using open framework materials, *Chem. Rev.*, 2020, **120**, 8581–8640.
8 M. Zhang, M. Lu, Z. L. Lang, J. Liu, M. Liu, J. N. Chang, L. Y. Li, L. J. Shang, M. Wang, S. L. Li and Y. Q. Lan, Semiconductor/covalent-organic-framework Z-scheme heterojunctions for artificial photosynthesis, *Angew. Chem.*, 2020, **132**, 6562–6568.
9 Y. Xiao, K. Wang, W. Dong and L. Li, Molecular engineering in tunable crystallinity of 2D covalent organic frameworks for efficient photocatalytic hydrogen evolution, *Polymer*, 2024, **300**, 126980.
10 C. Qian, L. Feng, W. L. Teo, J. Liu, W. Zhou, D. Wang and Y. Zhao, Imine and imine-derived linkages in two-dimensional covalent organic frameworks, *Nat. Rev. Chem.*, 2022, **6**, 881–898.
11 S. Ge, K. Wei, W. Peng, R. Huang, E. Akinlabi, H. Xia, M. W. Shahzad, X. Zhang, B. B. Xu and J. Jiang, A comprehensive review of covalent organic frameworks (COFs) and their derivatives in environmental pollution control, *Chem. Soc. Rev.*, 2024, **53**, 11259–11302.
12 M. Torabi, M. Yarie, A. Tavassoli, N. Zarei, L. Vatannavaz, M. A. Zolfigol, S. Azizian and S. Khazalpour, Heterocyclic-linked covalent organic frameworks: design, synthesis and applications, *Coord. Chem. Rev.*, 2025, **527**, 216359–216417.
13 S. Gopi and M. Kathiresan, 1,4-Phenylenediamine based covalent triazine framework as an electro catalyst, *Polymer*, 2017, **109**, 315–320.
14 J. C. Wang, X. Kan, J. Y. Shang, H. Qiao and Y. B. Dong, Catalytic asymmetric synthesis of chiral covalent organic frameworks from prochiral monomers for heterogeneous asymmetric catalysis, *J. Am. Chem. Soc.*, 2020, **142**, 16915–16920.
15 M. Torabi, M. A. Zolfigol, N. Zarei, M. Yarie and S. Azizian, Engineering iodine decorated azo-bridged porous organic polymer: a brilliant catalyst for the preparation of 2,4,6-trisubstituted pyridines, *Polymer*, 2025, **317**, 127873–127886.
16 X. Kan, J. C. Wang and Y. B. Dong, Metalated covalent organic frameworks as efficient catalysts for multicomponent tandem reactions, *Chem. Commun.*, 2024, **60**, 6362–6374.

17 G. F. Liu, Z. W. Li, Z. J. Huang, Z. Zhou, Y. X. Li, A. Huang, Z. Cai, G. Ouyang, B. H. Ye and Y. B. Zhang, Rapid crystallization and versatile metalation of acetylhydrazone-linked covalent organic frameworks for heterogenous catalysis, *J. Am. Chem. Soc.*, 2025, **147**, 1840–1850.

18 Y. Li, J. M. Wang, J. L. Kan, F. Li, Y. Dong and Y. B. Dong, Combination of a metal-*N*-heterocyclic–carbene catalyst and a chiral aminocatalyst within a covalent organic framework: a powerful cooperative approach for relay asymmetric catalysis, *Inorg. Chem.*, 2022, **61**, 2455–2462.

19 M. Torabi, M. A. Zolfigol and M. Yarie, Construction of a new 2D coral-like covalent organic framework as CuI nanoparticles carrier for the preparation of diverse triazoles, *Arabian J. Chem.*, 2023, **16**, 105090–105104.

20 J. Liu, H. Zhan, N. Wang, Y. Song, C. Wang, X. Wang, L. Ma and L. Chen, Palladium nanoparticles on covalent organic framework supports as catalysts for Suzuki–Miyaura cross-coupling reactions, *ACS Appl. Nano Mater.*, 2021, **4**, 6239–6249.

21 M. Bayatani, M. Torabi, M. Yarie, M. A. Zolfigol and Z. Farajzadeh, Fabrication of an imidazolium-based magnetic ionic porous organic polymer for efficient heterogeneous catalysis of Betti reaction, *J. Mol. Liq.*, 2023, **390**, 122863–122871.

22 M. Sedaghat, F. Moeinpour and F. S. Mohseni-Shahri, Copper(II)/polyimide linked covalent organic framework as a powerful catalyst for the solvent-free microwave irradiation-based synthesis of 2,4,5-trisubstituted imidazoles, *Anal. Sci. Adv.*, 2023, **4**, 302–311.

23 Y. Han, M. Zhang, Y. Q. Zhang and Z. H. Zhang, Copper immobilized at a covalent organic framework: an efficient and recyclable heterogeneous catalyst for the Chan–Lam coupling reaction of aryl boronic acids and amines, *Green Chem.*, 2018, **20**, 4891–4900.

24 H. J. Feng, X. Sun and J. W. Wang, A novel COF-based Cu heterogeneous catalyst for a green Suzuki cross-coupling reaction under mild conditions, *New J. Chem.*, 2023, **47**, 3104–3111.

25 M. Soleiman-Beigi, M. Mohammadi and H. Kohzadi, An overview on copper in industrial chemistry: from ancient pigment to modern catalysis, *Coord. Chem. Rev.*, 2025, **529**, 216438–216469.

26 M. Mohammadi, M. Khodamorady, B. Tahmasbi, K. Bahrami and A. Ghorbani-Choghamarani, Boehmite nanoparticles as versatile support for organic–inorganic hybrid materials: synthesis, functionalization, and applications in eco-friendly catalysis, *J. Ind. Eng. Chem.*, 2021, **97**, 1–78.

27 M. Borzooei, M. Norouzi and M. Mohammadi, Hyperbranched Polysiloxane-Copper (II) Pyridylamine-Glycidoxypropyltrimethoxysilane Complex-Catalyzed Click Reactions under Mild Conditions, *ACS Omega*, 2025, **10**, 21419–21431.

28 S. Beiranvand, M. Norouzi, M. Mohammadi and B. Tahmasbi, A New Dendrimer/Copper (II) Complex Supported on Hercynite Magnetic Nanoparticles: An Efficient Catalyst for the Synthesis of Tetrazoles, *J. Alloys Compd.*, 2025, **1035**, 181306–181318.

29 J. Duan, W. Wang, D. Zou, J. Liu, N. Li, J. Weng, L. Xu, Y. Guan, Y. Zhang and P. Zhou, Construction of a few-layered COF@CNT composite as an ultrahigh rate cathode for low-cost K-ion batteries, *ACS Appl. Mater. Interfaces*, 2022, **14**, 31234–31244.

30 Y. Quan, Y. Yang, Q. Liu and K. Börjesson, The effect of the oxidation level of graphene oxide substrate on *in situ* growth of COF-300, *Mater. Adv.*, 2025, **6**, 1744–1754.

31 Q. Niu, S. Dong, J. Tian, G. Huang, J. Bi and L. Wu, Rational design of novel COF/MOF S-scheme heterojunction photocatalyst for boosting CO_2 reduction at gas–solid interface, *ACS Appl. Mater. Interfaces*, 2022, **14**, 24299–24308.

32 B. P. Biswal, H. A. Vignolo-González, T. Banerjee, L. Grunenberg, G. Savasci, K. Gottschling, J. Nuss, C. Ochsenfeld and B. V. Lotsch, Sustained solar H_2 evolution from a thiazolo-[5,4-*d*]thiazole-bridged covalent organic framework and nickelthiolate cluster in water, *J. Am. Chem. Soc.*, 2019, **141**, 11082–11092.

33 X. Tan, R. Wu, Q. Zhu, Q. Gou, Y. Zhang, H. Huang and L. Fu, Pd nanoparticles anchored on carbon nanotubes/covalent organic frameworks for catalytic ethanol electrooxidation, *ACS Appl. Nano Mater.*, 2022, **5**, 597–604.

34 X. Sun, Y. Hu, Y. Fu, J. Yang, D. Song, B. Li, W. Xu and N. Wang, Single Ru sites on covalent organic framework-coated carbon nanotubes for highly efficient electrocatalytic hydrogen evolution, *Small*, 2024, **20**, 2305978–2305986.

35 J. Zhang, Y. Wang, M. Hong, B. Peng, C. Bao, X. Xu, D. Li, J. Chen, B. Wang and Q. Zhang, Ferrocene-based resin as heterogeneous fenton-like catalyst for efficient treatment of high salinity wastewater at acidic, neutral, and basic pH, *J. Chem. Eng.*, 2023, **464**, 142450–142460.

36 C. Wang, H. Zhou, S. Wen, Z. Chen, Y. Du, L. Shi and B. Li, Metallocene-based covalent metal-organic porous polymers and their derivatives, *Mater. Des.*, 2023, **225**, 111547–111558.

37 J. Sun, L. Shi, N. Wang, C. Miao, X. Xu, J. Yang, J. Wang and B. Zhou, A biodegradable ferrocene-based covalent organic framework as self-gated carrier for controlled drug delivery towards synergetic cancer enzymatic and chemical therapies, *J. Drug Delivery Sci. Technol.*, 2023, **87**, 104881–104889.

38 S. Kramer, N. R. Bennedsen and S. Kegnæs, Porous organic polymers containing active metal centers as catalysts for synthetic organic chemistry, *ACS Catal.*, 2018, **8**, 6961–6982.

39 B. Zhou, L. Liu, P. Cai, G. Zeng, X. Li, Z. Wen and L. Chen, Ferrocene-based porous organic polymer derived high-performance electrocatalysts for oxygen reduction, *J. Mater. Chem. A*, 2017, **5**, 22163–22169.

40 Y. Yang and Z. Lai, Ferrocene-based porous organic polymer for photodegradation of methylene blue and high iodine capture, *Microporous Mesoporous Mater.*, 2021, **316**, 110929–110937.

41 (*a*) J. Safaei Ghomi, S. Zahedi and M. A. Ghasemzadeh, AgI nanoparticles as a remarkable catalyst in the synthesis of (amidoalkyl) naphthol and oxazine derivatives: an eco-

friendly approach, *Monatsh. Chem.*, 2014, **145**, 1191–1199; (*b*) M. A. Ghasemzadeh and F. Ghaffarian, Preparation of core/shell/shell $CoFe_2O_4$/OCMC/Cu (BDC) nanostructure as a magnetically heterogeneous catalyst for the synthesis of substituted xanthenes, quinazolines and acridines under ultrasonic irradiation, *Appl. Organomet. Chem.*, 2020, **34**, e5580; (*c*) M. H. Abdollahi-Basir, B. Mirhosseini-Eshkevari, F. Zamani and M. A. Ghasemzadeh, Synthesis of tetrazolo [1,5-*a*] pyrimidine-6-carbonitriles using HMTA-BAIL@MIL-101(Cr) as a superior heterogeneous catalyst, *Sci. Rep.*, 2021, **11**, 5109.

42 K. Ishihara, T. Shioiri and M. Matsugi, An expeditious approach to tetrazoles from amides utilizing phosphorazidates, *Org. Lett.*, 2020, **22**, 6244–6247.

43 C. G. Neochoritis, T. Zhao and A. Domling, Tetrazoles via multicomponent reactions, *Chem. Rev.*, 2019, **119**, 1970–2042.

44 U. B. Patil, K. R. Kumthekar and J. M. Nagarkar, A novel method for the synthesis of 5-substituted 1*H*-tetrazole from oxime and sodium azide, *Tetrahedron Lett.*, 2012, **53**, 3706–3709.

45 R. Vishwakarma, C. Gadipelly and L. K. Mannepalli, Advances in tetrazole synthesis – an overview, *ChemistrySelect*, 2022, **7**, e202200706.

46 N. Verma, S. Bera and D. Mondal, Synthesis of tetrazole derivatives through conversion of amide and thioamide functionalities, *Chem. Heterocycl. Compd.*, 2022, **58**, 73–83.

47 M. Kazemnejadi, B. Mahmoudi, Z. Sharafi, M. A. Nasseri, A. Allahresani and M. Esmaeilpour, Copper coordinated-poly (α-amino acid) decorated on magnetite graphene oxide as an efficient heterogeneous magnetically recoverable catalyst for the selective synthesis of 5-and 1-substituted tetrazoles from various sources: a comparative study, *Appl. Organomet. Chem.*, 2020, **34**, e5273.

48 V. Rama, K. Kanagaraj and K. Pitchumani, Syntheses of 5-substituted 1*H*-tetrazoles catalyzed by reusable CoY zeolite, *J. Org. Chem.*, 2011, **76**, 9090–9095.

49 K. Ishihara, M. Kawashima, T. Shioiri and M. Matsugi, Synthesis of 5-substituted 1*H*-tetrazoles from aldoximes using diphenyl phosphorazidate, *Synlett*, 2016, **27**, 2225–2228.

50 M. Y. Xiao, M. M. Zheng, X. Peng, X. S. Xue and F. G. Zhang, Catalytic direct construction of cyano-tetrazoles, *Org. Lett.*, 2020, **22**, 7762–7767.

51 (*a*) Y. Lu, Y. Fu, Z. Hu, S. Feng, M. Torabi, L. Gao, S. Fu, Z. Wang, C. Huang, X. Huang, M. Wang, N. Israel, E. Dmitrieva, H. I. Wang, M. Bonn, P. Samorì, R. Dong, E. Coronado and X. Feng, Rational construction of layered two-dimensional conjugated metal–organic frameworks with room-temperature quantum coherence, *J. Am. Chem. Soc.*, 2025, **147**, 8778–8784; (*b*) Z. Alishahi, M. Torabi, M. A. Zolfigol and M. Yarie, Nanoarchitectonics of magnetic covalent organic framework with sulfonic acid tags for catalytic preparation of triazolo quinazolinones and 4*H*-pyrimidobenzothiazoles, *J. Solid State Chem.*, 2023, **324**, 124119; (*c*) E. Abdoli, M. Torabi, M. Yarie and M. A. Zolfigol, Magnetic covalent organic framework with ionic tags as an efficient catalyst in the preparation of 2,3-disubstituted thiazolidine-4-ones and *N*-amino-2-pyridones, *Arabian J. Chem.*, 2024, **17**, 105908–105923; (*d*) M. Torabi, M. Yarie, M. A. Zolfigol, S. Azizian and Y. Gu, A magnetic porous organic polymer: catalytic application in the synthesis of hybrid pyridines with indole, triazole and sulfonamide moieties, *RSC Adv.*, 2022, **12**, 8804–8814; (*e*) R. Zandipak, N. Bahramifar, M. Torabi, M. Calero, M. J. Muñoz-Batista and R. R. Solís, Synergistic effect of graphitic-like carbon nitride and sulfur-based thiazole-linked organic polymer heterostructures for boosting the photocatalytic degradation of pharmaceuticals in water, *Chem. Eng. J.*, 2024, **494**, 152843–152859; (*f*) N. Zarei, M. Yarie, M. Torabi and M. A. Zolfigol, Urea-rich porous organic polymer as a hydrogen bond catalyst for Knoevenagel condensation reaction and synthesis of 2,3-dihydroquinazolin-4(1*H*)-ones, *RSC Adv.*, 2024, **14**, 1094–1105; (*g*) M. Torabi, Catalytic applications of porous organic polymers, *Iran. J. Catal.*, 2021, **11**, 417–424; (*h*) M. Torabi, S. Azizian and M. A. Zolfigol, Enhanced interfacial solar steam generation using a perylene-based covalent organic framework coupled with VO_2, *Chem. Eng. J.*, 2025, **520**, 166258–166270; (*i*) Z. Alishahi, Hybrid reticular chemistry-based catalysis, *Iran. J. Catal.*, 2025, DOI: **10.57647/j.ijc.2025.1503.38**.

52 Y. Wang, J. Tao, S. Xiong, P. Lu, J. Tang, J. He, M. U. Javaid and C. P. G. Yu, Ferrocene-based porous organic polymers for high-affinity iodine capture, *J. Chem. Eng.*, 2020, **380**, 122420–122425.

53 M. M. Samy, M. G. Mohamed and S. W. Kuo, Conjugated microporous polymers based on ferrocene units as highly efficient electrodes for energy storage, *Polymers*, 2023, **15**, 1095–1100.

54 L. L. Zhou, Q. Guan, W. Y. Li, Z. Zhang, Y. A. Li and Y. B. Dong, A ferrocene-functionalized covalent organic framework for enhancing chemodynamic therapy *via* redox dyshomeostasis, *Small*, 2021, **17**, 2101368–2101380.

55 (*a*) B. Akhlaghinia and S. Rezazadeh, A novel approach for the synthesis of 5-substituted-1*H*-tetrazoles, *J. Braz. Chem. Soc.*, 2012, **23**, 2197–2203; (*b*) P. Mani, A. K. Singh and S. K. Awasthi, $AgNO_3$ catalyzed synthesis of 5-substituted-1*H*-tetrazole via [3+2] cycloaddition of nitriles and sodium azide, *Tetrahedron Lett.*, 2014, **55**, 1879–1882.

56 J. Hasani, M. Ghadermazi and S. Molaei, Ni (II) supported ordered mesoporous cobalt ferrite as a novel, efficient, and reusable heterogeneous catalyst for the synthesis of 5-substituted 1*H*-tetrazoles in green media, *Res. Chem. Intermed.*, 2024, **50**, 3665–3686.

57 M. R. Bhosle, D. S. Shaikh, L. D. Khillare, A. R. Deshmukh and R. A. Mane, Diisopropylethylammonium acetate (DIPEAc): an efficient and recyclable catalyst for the rapid synthesis of 5-substituted-1*H*-tetrazoles, *Synth. Commun.*, 2017, **47**, 695–703.

58 I. Fatima, H. Zafar, K. M. Khan, S. M. Saad, S. Javaid, S. Perveen and M. I. Choudhary, Synthesis, molecular docking and xanthine oxidase inhibitory activity of 5-aryl-1*H*-tetrazoles, *Bioorg. Chem.*, 2018, **79**, 201–211.

59 S. K. Prajapti, A. Nagarsenkar and B. N. Babu, An efficient synthesis of 5-substituted 1*H*-tetrazoles via $B(C_6F_5)_3$ catalyzed [3+2] cycloaddition of nitriles and sodium azide, *Tetrahedron Lett.*, 2014, **55**, 3507–3510.

60 R. Singh and N. Ahmed, Direct one-pot synthesis of tetrazole derivatives from aldehydes under metal-free conditions, *Synlett*, 2024, **36**, 1003–1008.

61 H. Käsnänen, M. J. Myllymäki, A. Minkkilä, A. O. Kataja, S. M. Saario, T. Nevalainen, A. M. P. Koskinen and A. Poso, 3-Heterocycle-phenyl *N*-alkylcarbamates as FAAH inhibitors: design, synthesis and 3D-QSAR studies, *ChemMedChem*, 2010, **5**, 213–231.

62 H. Yoneyama, M. Adachi, A. Morita, M. Nakagawa, M. Baba, K. Yamawaki, N. Hayama, S. Harusawa and Y. Usami, Synthesis of 5,6-dihydro-4*H*-pyrrolo [1,2-*b*] pyrazoles and homologs from 5-substituted 2-(alkynyl) tetrazoles via microwave-induced intramolecular nitrile-imine–alkyne 1,3-dipolar cycloaddition, *Synthesis*, 2023, **55**, 945–958.

63 Y. Zhang, Construction and characterization of Fe_3O_4@SiO_2-Dop/Amide-BTA-pd(0) nanocomposite as a novel and efficient nanomagnetic recoverable catalyst for synthesis of 5-substituted 1*h*-tetrazoles in water, *J. Coord. Chem.*, 2024, **77**, 2076–2097.

64 S. S. A. Darbandizadeh Mohammad Abadi and M. A. K. Zarchi, A novel route for the synthesis of 5-substituted 1-*H* tetrazoles in the presence of polymer-supported palladium nanoparticles, *New J. Chem.*, 2017, **41**, 10397–10406.

65 A. N. Parouch and N. Koukabi, Facile synthesis of multifunctional magnetic porous organic polymers with high catalytic performance and dye adsorption capacity, *New J. Chem.*, 2024, **48**, 3646–3655.

66 F. Pirani, H. Eshghi and S. A. Rounaghi, Immobilized Cu(0) nanoparticles on montmorillonite-modified with benzalkonium chloride (MMT-BAC@Cu(0)): as an eco-friendly and proficient heterogeneous nano-catalyst for green synthesis of 5-substituted 1*H*-tetrazoles, *RSC Adv.*, 2023, **13**, 6160–6170.

67 S. Bondarian, M. G. Dekamin, E. Valiey, M. R. Naimi-Jamal and M. R. Naimi-Jamal, Supramolecular Cu(ii) nanoparticles supported on a functionalized chitosan containing urea and thiourea bridges as a recoverable nanocatalyst for efficient synthesis of 1*H*-tetrazoles, *RSC Adv.*, 2023, **13**, 27088–27105.

68 M. Bakherad, R. Doosti, A. Keivanloo, M. Gholizadeh and K. Jadidi, Rapid, green, and catalyst-free one-pot three-component syntheses of 5-substituted 1*H*-tetrazoles in magnetized water, *J. Iran. Chem. Soc.*, 2017, **14**, 2591–2597.

69 A. N. Parouch and N. Koukabi, Facile synthesis of multifunctional magnetic porous organic polymers with high catalytic performance and dye adsorption capacity, *New J. Chem.*, 2024, **48**, 3646–3655.

70 A. Vignesh, N. S. Bhuvanesh and N. Dharmaraj, Conversion of arylboronic acids to tetrazoles catalyzed by ONO pincer-type palladium complex, *J. Org. Chem.*, 2017, **82**, 887–892.

71 G. Vinoth, S. Indira, M. Bharathi, G. Archana, L. G. Alves, A. M. Martins and K. S. Bharathi, Catalytic conversion of 2,4,5-trisubstituted imidazole and 5-substituted 1*H*-tetrazole derivatives using a new series of half-sandwich (η^6-*p*-cymene) ruthenium (II) complexes with thiophene-2-carboxylic acid hydrazone ligands, *Inorg. Chim. Acta*, 2021, **516**, 120089–120099.

72 N. Nowrouzi, S. Farahi and M. Irajzadeh, Piperazinium Dihydrogen Sulfate: An Acidic Ionic Liquid for the [3+2] Cycloaddition Reaction of Sodium Azide with Organic Nitriles, *Lett. Org. Chem.*, 2016, **13**, 113–119.

73 M. A. Zolfigol, S. Azizian, M. Torabi, M. Yarie and B. Notash, The importance of nonstoichiometric ratio of reactants in organic synthesis, *J. Chem. Educ.*, 2024, **101**, 877–881.